AIP | Physics of Plasmas

A spectral method for halo particle definition in intense mismatched beams

Mikhail A. Dorf, Ronald C. Davidson, and Edward A. Startsev

Citation: Phys. Plasmas **18**, 043109 (2011); doi: 10.1063/1.3574665
View online: http://dx.doi.org/10.1063/1.3574665
View Table of Contents: http://pop.aip.org/resource/1/PHPAEN/v18/i4
Published by the American Institute of Physics.

A spectral method for halo particle definition in intense mismatched beams

Mikhail A. Dorf,[a] Ronald C. Davidson, and Edward A. Startsev
Plasma Physics Laboratory, Princeton, New Jersey 08543, USA

(Received 15 December 2010; accepted 10 March 2011; published online 28 April 2011)

An advanced spectral analysis of a mismatched charged particle beam propagating through a periodic focusing transport lattice is utilized in particle-in-cell (PIC) simulations. It is found that the betatron frequency distribution function of a mismatched space-charge-dominated beam has a bump-on-tail structure attributed to the beam halo particles. Based on this observation, a new spectral method for halo particle definition is proposed that provides the opportunity to carry out a quantitative analysis of halo particle production by a beam mismatch. In addition, it is shown that the spectral analysis of the mismatch relaxation process provides important insights into the emittance growth attributed to the halo formation and the core relaxation processes. Finally, the spectral method is applied to the problem of space-charge transport limits. © *2011 American Institute of Physics*. [doi:10.1063/1.3574665]

I. INTRODUCTION

The production and control of high-energy halo particles ejected from the beam core is a critical problem in intense charge particle beam propagation through a periodic focusing lattice.[1] One of the typical mechanisms of the halo particle production is a mechanism in which halo particles gain energy by means of parametric resonant interaction with the collective self-field perturbations produced by a beam mismatch (mismatch oscillations).[2–11] More specifically, due to the nonlinear transverse dependence of the beam self-fields near and beyond the beam edge, individual beam particles can oscillate about and through the beam core with energy-dependent *betatron* frequency. Collective self-field mismatch oscillations produce modulation of the betatron frequency and, therefore, parametric resonant interaction between the edge beam particles and the collective modes may occur. In particular, beam particles, which are close to the fundamental 2:1 resonance with the collective mismatch oscillation, can gain transverse energy and populate the halo region.[2]

Although, the presence of a beam halo is typically evident by visual inspection of the mismatched beam distribution, it is of particular interest to obtain a more quantitative measure of this phenomena.[9–11] In Ref. 10, the *beam profile parameter* constructed from the second and fourth spatial moments of the beam distribution,

$$h_i = \frac{\langle q_i^4 \rangle}{\langle q_i^2 \rangle^2} - 2,$$

has been proposed as a characterization of the halo in a 1D spatial projection. Here, q_i is the transverse particle coordinate of the ith phase plane, and $\langle \cdots \rangle$ denotes the average over the particle distribution function. This formalism for calculating dimensionless halo parameters, based upon moments of the beam distribution function, has been then extended to quantify halo formation in 2D phase space.[11] The phase-space *halo parameter*,[11]

$$H_i = \frac{\sqrt{3\langle q_i^4 \rangle \langle p_i^4 \rangle + 9\langle q_i^2 p_i^2 \rangle^2 - 12\langle q_i p_i^3 \rangle \langle p_i q_i^3 \rangle}}{2\langle q_i^2 \rangle \langle p_i^2 \rangle - 2\langle q_i p_i \rangle^2} - 2,$$

is a generalization of the spatial-profile parameter h_i, using kinematic invariants of the particle distribution in phase space. Here, p_i corresponds to the transverse particle momentum of the ith phase plane. These halo parameters can be efficiently used for comparing the "halo intensity" for different beam distributions. For instance, it follows that $h_i = H_i = 0$ for the Kapchinskij–Vladimirskij distribution, and $h_i = H_i = 1$ for a Gaussian distribution in phase-space coordinates.

Although the evolution of the halo parameters (h_i, H_i) can provide important insights into the halo production process, no guidelines have been provided on how to quantitatively distinguish halo particles from core particles. Therefore, the actual "halo fraction" of all beam particles for a given distribution cannot be readily estimated. Attempts to distinguish halo particles from the beam core particles were made in Refs. 7 and 8. However, those studies were based on a "visual analysis" of the transverse phase space, and no rigorous mathematical criteria were applied.

A simple quantitative definition of halo particles based on an analysis of the beam betatron frequency distribution has been outlined in Ref. 9, where it was demonstrated that the betatron frequency distribution function of an intense mismatched space-charge-dominated beam has a well-defined bump-on-tail structure attributed to the beam halo particles. In this paper, we develop a detailed framework for this spectral method. In addition, we extend the definition of halo particles to a broad range of beam intensities. Finally, we show that the spectral analysis can also provide important insights into other critical problems in intense beam transport, e.g., mismatch relaxation processes, and space-charge transport limits.[12–14]

This paper is organized as follows. The theoretical model describing the transverse beam dynamics is

[a]Present address: Lawrence Livermore National Laboratory, Livermore, California 94550, USA.

summarized in Sec. II. In Sec. III, we describe the spectral method, making use of the smooth-focusing approximation, and in Sec. IV, we take into account the effects of an alternating-gradient quadrupole field. Finally, in Sec. V, the spectral method is applied to an analysis of the mismatch relaxation process, and space-charge transport limits.

II. THEORETICAL MODEL

In this section, we summarize the general theoretical models used to describe the nonlinear transverse dynamics of a charged particle beam propagating through an alternating-gradient quadrupole lattice. We consider a long coasting beam propagating through an alternating-gradient quadrupole lattice and perform the analysis of the transverse beam dynamics in the frame of reference moving with the beam. The applied focusing force of the periodic lattice is assumed to be of the form,

$$\mathbf{F}_{\mathrm{foc}} = -m_b \kappa_q(t)\left[x\hat{\mathbf{e}}_x - y\hat{\mathbf{e}}_y\right], \tag{1}$$

where $\kappa_q(t) = \hat{\kappa}_q \sin(2\pi t/\tau_L)$ is the lattice function, τ_L is the lattice period, m_b is the particle mass, and $(x, y, \dot{x}, \dot{y})$ is the transverse beam phase space. For the case where the beam distribution function is close to a beam quasiequilibrium, the evolution of the characteristic transverse beam dimensions $\bar{a}(t) = 2\langle x^2\rangle^{1/2}$ and $\bar{b}(t) = 2\langle y^2\rangle^{1/2}$ can be described approximately by the simplified envelope equations[1,15]

$$\frac{d^2}{dt^2}\bar{a} + \left[\kappa_q(t) - \frac{2K_b}{\bar{a}(\bar{a}+\bar{b})}\right]\bar{a} = \frac{\varepsilon^2}{\bar{a}^3}, \tag{2}$$

$$\frac{d^2}{dt^2}\bar{b} + \left[-\kappa_q(t) - \frac{2K_b}{\bar{b}(\bar{a}+\bar{b})}\right]\bar{b} = \frac{\varepsilon^2}{\bar{b}^3}. \tag{3}$$

Here, $K_b = 2N_b e_b^2/m_b$ is the beam self-field perveance, $N_b = \int dxdyd\dot{x}d\dot{y}f_b$ is the beam line density, e_b is the particle charge, and we have assumed $\varepsilon_x = \varepsilon_y \equiv \varepsilon$, where the transverse emittance ε_x, is defined by

$$\varepsilon_x = 4\sqrt{\langle(x-\langle x\rangle)^2\rangle\langle(\dot{x}-\langle\dot{x}\rangle)^2\rangle - \langle(x-\langle x\rangle)(\dot{x}-\langle\dot{x}\rangle)\rangle^2}, \tag{4}$$

and, $\langle\chi\rangle = N_b^{-1}\int dxdyd\dot{x}d\dot{y}\chi f_b$ denotes the statistical average of a phase function χ over the beam distribution function, f_b. The matched solutions to the envelope Eqs. (2) and (3), satisfying $\bar{a}(t+\tau_L) = \bar{a}(t)$ and $\bar{b}(t+\tau_L) = \bar{b}(t)$, can be used for calculation of the *phase advances*.[1] The vacuum phase advance σ_v, describing the normalized lattice strength, can be expressed as

$$\sigma_v \equiv \lim_{K_b\to 0}\varepsilon\int_{t_0}^{t_0+\tau_L}\frac{dt}{\bar{a}^2(t)} = \lim_{K_b\to 0}\varepsilon\int_{t_0}^{t_0+\tau_L}\frac{dt}{\bar{b}^2(t)}, \tag{5}$$

and the depressed phase advance σ, including self-field effects, is given by

$$\sigma_v \equiv \varepsilon\int_{t_0}^{t_0+\tau_L}\frac{dt}{\bar{a}^2(t)} = \varepsilon\int_{t_0}^{t_0+\tau_L}\frac{dt}{\bar{b}^2(t)}. \tag{6}$$

Note that the ratio σ/σ_v can be used as a normalized measure of the space-charge strength, with $\sigma/\sigma_v \to 1$ corresponding to an emittance-dominated beam with negligible space-charge force, and $\sigma/\sigma_v \to 0$ corresponding to a space-charge-dominated beam with negligible emittance.

In order to describe the average beam dynamics, the smooth-focusing approximation is often used, in which the applied focusing force in Eq. (1) is replaced by the uniform focusing force,

$$\mathbf{F}_{\mathrm{foc}}^{sf} = -m_b\omega_q^2\left(x\hat{\mathbf{e}}_x + y\hat{\mathbf{e}}_y\right). \tag{7}$$

Here, the smooth-focusing frequency ω_q is related to the amplitude of the sinusoidal lattice function $\hat{\kappa}_q$ (approximately) by $\hat{\kappa}_q = 2^{3/2}\pi\omega_q\tau_L^{-1}$.[1] In the smooth-focusing approximation, the envelope Eqs. (2) and (3) have same form, but the terms describing the oscillating force of the quadrupole lattice, i.e., $\kappa_q(t)$ in Eq. (2) and $-\kappa_q(t)$ in Eq. (3), are replaced with the term $+\omega_q^2$ corresponding to the smooth-focusing lattice coefficient. For the case of an azimuthally symmetric beam, it is straightforward to show that the matched smooth-focusing solutions are given by $\bar{a}(s) = \bar{b}(s) = \sqrt{2}R_{b0}$, where R_{b0} is determined from

$$\left(\omega_q^2 - \frac{K_b}{2R_{b0}^2}\right)R_{b0} = \frac{\varepsilon^2}{4R_{b0}^3}, \tag{8}$$

and the smooth-focusing phase advances are given approximately by[1]

$$\sigma_v^{sf} = \omega_q\tau_L \tag{9}$$

and

$$\frac{\sigma^{sf}}{\sigma_v^{sf}} = \left[1 + \left(\frac{K_b}{2\varepsilon\omega_q}\right)^2\right]^{1/2} - \frac{K_b}{2\varepsilon\omega_q}. \tag{10}$$

Finally, we point out that along with $\sigma^{sf}/\sigma_v^{sf}$, the normalized beam intensity can be characterized by the dimensionless parameter $s_b = \omega_{pb}^2/2\omega_q^2$, where $\omega_{pb} = \left(4\pi e_b^2 n_0/m_b\right)^{1/2}$ is the plasma frequency, and n_0 is the on-axis number density.[1]

The envelope Eqs. (2) and (3) describing the evolution of the beam transverse dimensions support mismatch oscillations around a beam quasiequilibrium. In the smooth-focusing approximation, it is straightforward to show that the oscillation frequencies of these normal modes are given by

$$\omega_s^{sf} = \left(K_b/R_{b0}^2 + \varepsilon^2/R_{b0}^4\right)^{1/2}, \tag{11}$$

$$\omega_{\mathrm{odd}}^{sf} = \left(K_b/2R_{b0}^2 + \varepsilon^2/R_{b0}^4\right)^{1/2}, \tag{12}$$

where the rms beam radius, R_{b0}, is determined from Eq. (8). Here, ω_s^{sf} corresponds to the symmetric (even) mode with $\delta\bar{a} = \delta\bar{b}$, and $\omega_{\mathrm{odd}}^{sf}$ corresponds to the quadrupole (odd) mode with $\delta\bar{a} = -\delta\bar{b}$, where $\delta\bar{a}$ and $\delta\bar{b}$ are the small-signal perturbations of the transverse matched-beam dimensions $\bar{a}$ and $\bar{b}$, respectively. The quadrupole and symmetric modes represent collective transverse oscillations of the charged particle beam envelope. On the other hand, due to the nonlinear transverse dependence of the beam self-fields near and beyond the beam edge, individual beam particles can oscillate about and through the beam core with energy-

dependent *betatron* frequency. Collective self-field perturbations produce modulation of the betatron frequency and, therefore, parametric resonant interaction between the edge beam particles and the collective modes may occur. In particular, beam particles, which are close to fundamental resonance with the collective mismatch oscillation, can gain transverse energy and populate the halo region.

III. SMOOTH-FOCUSING APPROXIMATION

This section develops a framework for the quantitative analysis of halo production by a beam mismatch, making use of the smooth-focusing approximation, which describes the average focusing effect of the oscillating confining field. As noted earlier, in order to describe the production of halo particles by a beam mismatch, it is convenient to consider a beam propagating through a periodic focusing lattice as an ensemble of betatron oscillators coupled to the collective mismatch oscillations. This approach was also used in Refs. 16 and 17 for the analysis of beam mismatch relaxation for the case of a quadrupole lattice. It was pointed out[16,17] that for the case of a space-charge-dominated beam, most of the betatron oscillators in the initial beam equilibrium distribution are far from the parametric (2:1) resonance with the collective mismatch mode. Therefore, only a slight damping of the collective oscillations occurs. However, as the beam space-charge intensity decreases, the half-value of the mismatch frequency approaches the frequency distribution of the betatron oscillators, providing an increased damping of the collective oscillations. As shown in Fig. 1, the beam betatron frequency distributions and the corresponding mismatch oscillation frequencies obtained for the smooth-focusing thermal equilibrium distribution[1] for various values of the beam intensity concur with the conclusions in Refs. 16 and 17. Inspecting Fig. 1, it is also instructive to note that as the beam intensity increases the beam frequency spectrum shifts toward lower frequency values relative to the smooth-focusing frequency, ω_q. This is consistent with the fact that

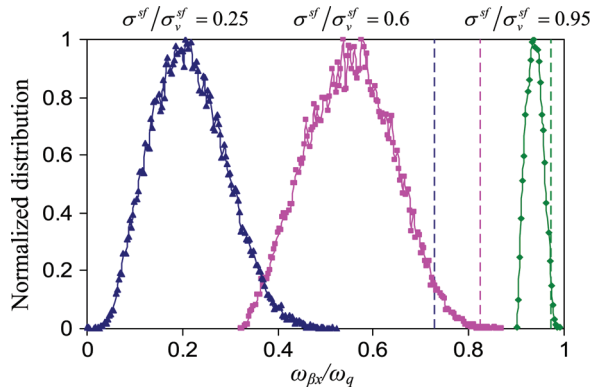

FIG. 1. (Color online) Plots of the normalized beam betatron frequency distribution for the smooth-focusing thermal equilibrium distribution obtained for different values of the beam intensity corresponding to $\sigma/\sigma_{vac} = 0.25$, $s_b = 0.9999$ (blue triangles), $\sigma/\sigma_{vac} = 0.6$, $s_b = 0.9$ (pink squares), $\sigma/\sigma_{vac} = 0.95$, $s_b = 0.2$ (green diamonds). Each frequency distribution is normalized to its maximum value. The vertical dashed lines show the corresponding half-values of the mismatch oscillations frequency obtained within the smooth-focusing approximation, $\omega_s^{sf}/2$. Results are obtained using the WARP PIC-code (Ref. 18) for a smooth-focusing field.

the beam self-fields depress the total focusing force acting on a beam particle and, therefore, increase the period of particle betatron oscillations. Also, note that the frequency spectrum width is attributed to the nonlinear effects of the beam self-fields. Therefore, for the case of the smooth-focusing thermal equilibrium distributions shown in Fig. 1, the spectrum width has a maximum for a moderate beam intensity. Indeed, as the beam intensity increases, the beam density profile approaches a flat-top distribution, and hence the self-electric fields become nearly linear. On the other hand, as the beam density decreases, the effects of the beam self-fields become less pronounced.[19] Without loss of generality, here and throughout the remainder of this paper, for illustrative purposes, we show the betatron frequency distributions corresponding to the particle oscillatory motion in the x-direction. Also, each plotted betatron frequency distribution is normalized to its maximum value. Finally, the number of macroparticles used in the simulations is $N_p = 40\ 000$, and typical grid resolution corresponds to 16 grid points across the beam cross-section.

In previous studies,[16,17] the spectral analysis was applied to the initial beam quasiequilibrium. Here, we extend the betatron spectral analysis to the case of a mismatched beam distribution. This allows us to develop a convenient framework for the quantitative analysis of halo production by a beam mismatch. Note that a particle betatron frequency increases with an increase in a particle energy. Therefore, the high-energy tail of an initial beam equilibrium distribution corresponds to the high-frequency tail in the betatron frequency distribution (Fig. 1). Inspecting the betatron frequency distribution of the initial beam thermal equilibrium distribution for the case of a space-charge-dominated beam, it is evident that only an exponentially small fraction of the beam particles has the energy corresponding to the parametrically resonant frequency, $\omega_s^{sf}/2$. However, during the relaxation of a large beam mismatch, there is an energy transfer from the collective mismatch modes to the resonant particles, which gain energy and populate the halo region. It is therefore intuitively appealing to expect that a "bump-on-tail" structure attributed to the high-energy halo particle will appear near the half-value of the mismatch oscillations frequency in the betatron frequency distribution of a *mismatched* space-charge-dominated beam.

Figure 2(a) shows the beam betatron frequency distribution for the case of a mismatched space-charge-dominated beam. For this illustrative example, a thermal equilibrium beam distribution[1] with $\sigma^{sf}/\sigma_v^{sf} = 0.25$ ($s_b = 0.9999$) was subjected to an instantaneous increase in the applied smooth-focusing force, $\omega_q^{inc}/\omega_q = 1.3$. Then, after a time period, $\tau_{step} = \pi/\left[2\left(\omega_s^{sf}\right)_i\right]$, corresponding to one-quarter of the linear mismatch oscillation period calculated for the initial beam equilibrium, the applied force is returned back to its initial value. Here, $\left(\omega_s^{sf}\right)_i = \left(K_b/R_{bi}^2 + \varepsilon_i^2/R_{bi}^4\right)^{1/2}$, $R_b = \langle x^2 + y^2\rangle^{1/2}$ is the rms beam radius, and the subscript "i" denotes the initial equilibrium beam state. This perturbation provides the initial beam mismatch $\mu = 2.2$ as measured by the ratio of the maximum to minimum values of R_b. Note that we have assumed an azimuthally symmetric initial beam distribution and, therefore, only the symmetric (even) mode of mismatch

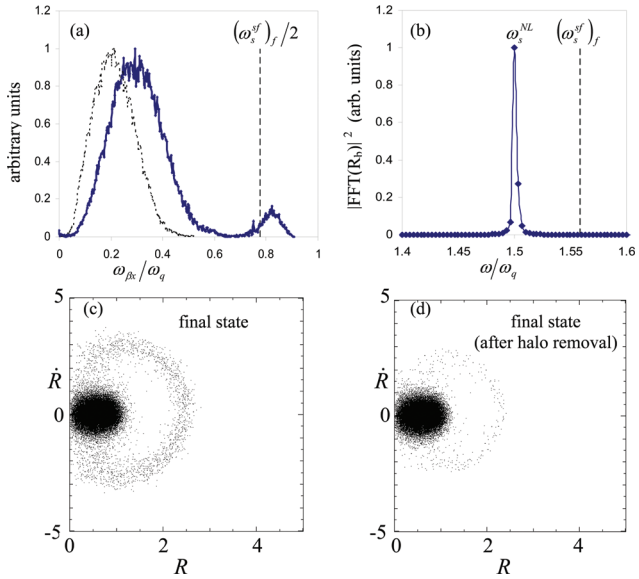

FIG. 2. (Color online) Relaxation of a beam mismatch for the case of a space-charge-dominated beam with $\sigma^{sf}/\sigma_v^{sf} = 0.25$, $s_b = 0.9999$. Shown are plots of (a) beam betatron frequency distribution for the final quasirelaxed state (solid blue curve) and for the initial state corresponding to the smooth-focusing thermal equilibrium distribution (dashed black curve), (b) FFT of $R_b(t)$, (c) and (d) the instantaneous $(\dot{R}, R)$ phase space corresponding to the final beam state at $t = 3300.42 \times 2\pi/\omega_q$, and the same state after halo removal, respectively. The amplitude of the mismatch oscillations in the final state is $\delta R_b/R_b \cong 0.12$, and the time interval used for the FFT calculations of the betatron frequency distribution in the final state corresponds to $(3000 \times 2\pi/\omega_q, 3300 \times 2\pi/\omega_q)$. Results are obtained using the WARP code for a smooth-focusing field.

oscillations is excited. After introducing the beam mismatch as described above, the beam is allowed to relax until the mismatch amplitude remains nearly constant.[8] In the final ("quasirelaxed") beam state, the x and y coordinates of each beam particle are tracked, and the fast-Fourier transform (FFT) averages of the particle oscillograms are calculated [Fig. 3(c)]. It should be noted that the single-particle motion for the case of a mismatched intense beam is, in general, nonintegrable, and the corresponding frequency spectra may have a complex structure [Fig. 3(c)]. Indeed, in addition to the fundamental (2:1) "halo" resonance, nonuniformities in the beam density profile along with the mismatch oscillations produce a higher-order resonance structure inside the beam core and, therefore, even the core particle motion can become chaotic (Fig. 3). For the construction of the beam betatron frequency distribution [Fig. 2(a)], the particle's "betatron" frequency is assigned to the frequency corresponding to the maximum value in the Fourier power spectrum of the particle oscillogram. As evident from Fig. 3, the power frequency spectra and particle oscillograms for typical core and halo particles elucidate the relevance of this approach for the purpose of distinguishing a halo particle from a core particle. Indeed, the betatron frequency values for the core and halo beam particles lie inside the "core" and bump-on-tail frequency ranges of the beam betatron frequency distribution, respectively [Fig. 2(a)]. The corresponding Poincare radial phase-space plots $(\dot{R}, R)$ for these halo and core particles are shown in Fig. 3(d). Here, $R \equiv \sqrt{X^2 + Y^2}$, $\dot{R} \equiv (\dot{X}X + \dot{Y}Y)/R$, X and $\dot{X}$ are the scaled coordinates defined as $X = x/\bar{a}$ and $\dot{X} = (\bar{a}\dot{x} - x\dot{\bar{a}})/\varepsilon_x$, and Y and $\dot{Y}$ are their analogs in the y-direction.

Figure 2(a) shows that the betatron frequency distribution function of a mismatched space-charge-dominated beam has a clear bump-on-tail structure attributed to beam halo particles. Note that most of the bump is located to the right of the half-value of the mismatch oscillation frequency calculated for the final beam distribution, $(\omega_s^{sf})_f = \left(K_b/R_{bf}^2 + \varepsilon_f^2/R_{bf}^4\right)^{1/2}$. Here, ε_f corresponds to the average value of the transverse beam emittance in the final state, and R_{bf} is the corresponding value

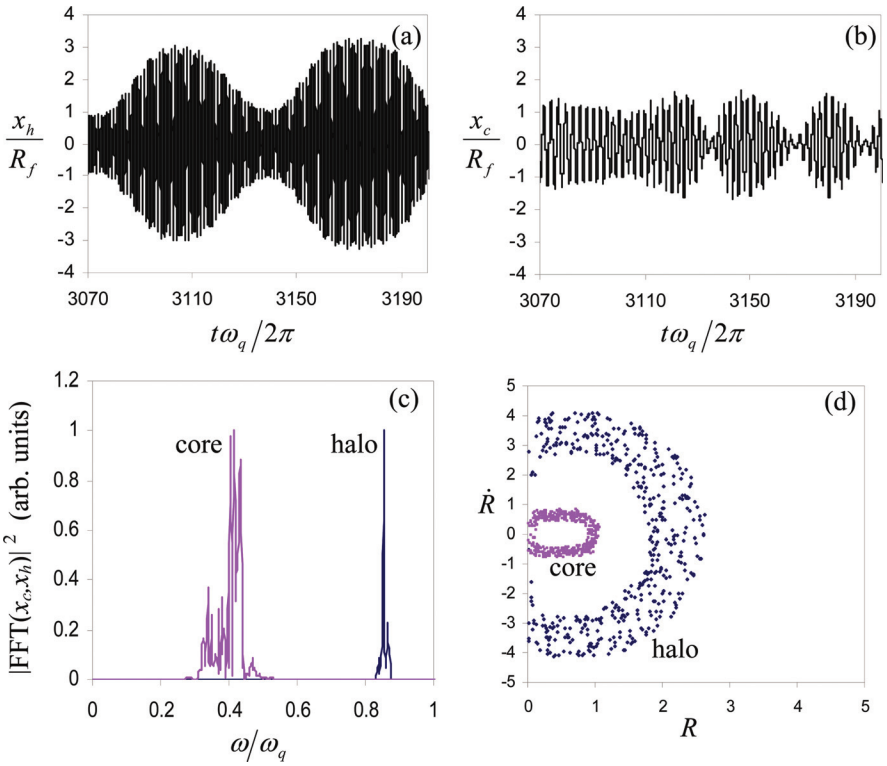

FIG. 3. (Color online) Dynamics of core and halo particles in the final state of a mismatched space-charge-dominated beam with $\sigma^{sf}/\sigma_v^{sf} = 0.25$ ($s_b = 0.9999$). (a) and (b) Normalized x/R_f-oscillogram of the halo and core particles motion, respectively. Here, R_f corresponds to the rms equilibrium radius calculated for the final beam state. (c) FFT of the core particle (pink) and the halo particle (blue) x-oscillograms. (d) Poincare section for the core (pink) and halo (blue) particles with the strobe time, taken at the minimum of the beam radius. Results are obtained using the WARP code for a smooth-focusing force. The parameters of the simulation are the same as in Fig. 2.

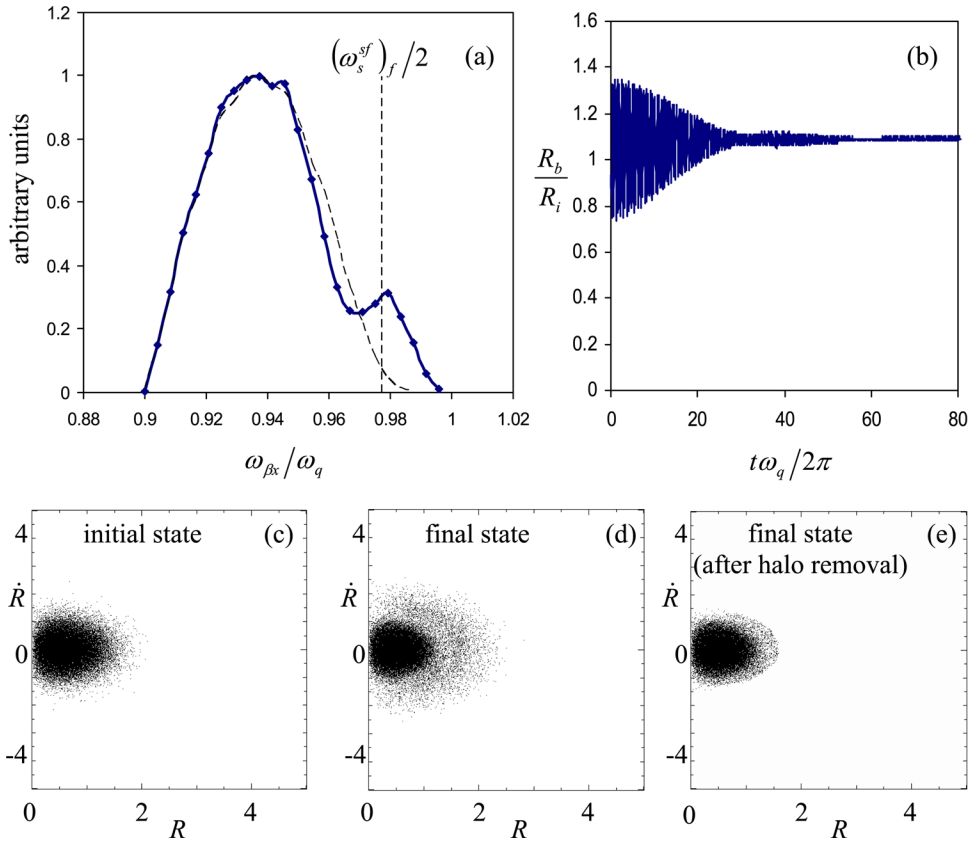

FIG. 4. (Color online) Relaxation of a beam mismatch for the case of an emittance-dominated beam with $\sigma^{sf}/\sigma_v^{sf} = 0.95$ ($s_b = 0.2$). Shown are plots of (a) beam betatron frequency distribution for the final "quasirelaxed" state (solid blue curve) and for the initial state corresponding to the smooth-focusing thermal equilibrium distribution (dashed black curve) and (b) the evolution of the normalized rms beam radius R_b/R_i. Frames (c), (d), and (e) show the normalized $(\dot{R}, R)$ phase space corresponding to the initial state, final state at $t = 540.46 \times 2\pi/\omega_q$, and final state after halo removal, respectively. The time interval used for the FFT calculations of the betatron frequency distribution in the final state corresponds to ($300 \times 2\pi/\omega_q$, $540 \times 2\pi/\omega_q$). Results are obtained using the WARP code for a smooth-focusing field.

of the rms equilibrium beam radius determined from Eq. (8) where $\varepsilon = \varepsilon_f$. This allows us to formulate the following simple quantitative definition of a halo particle. *If the particle betatron frequency is greater than one-half of the mismatch oscillation frequency then it is designated as a halo particle*. Figures 2(c) shows the beam radial phase space at the final state, and Fig. 2(d) shows the same phase space after removing particles with betatron frequency in the x or y direction higher than $(\omega_s^{sf})_f/2$. The remaining small fraction of halo particles corresponds to the fraction of the bump-on-tail structure located to the left of $(\omega_s^{sf})_f/2$. In addition, a few more halo particles appear during the FFT averaging calculations, because the energy transfer process is not yet fully completed. Note that the actual frequency spectrum of an envelope rms dimension [Fig. 3(b)] has a finite bandwidth with the central frequency ω_s^{NL}, which is slightly smaller than its linear approximation, $(\omega_s^{sf})_f$ due to nonlinear effects, and also due to the coupling to the dynamics of the higher-order moments, e.g., beam emittance. Therefore, more halo particles can be selected by the proposed criteria if an improved model for describing the mismatch oscillations frequency spectrum is employed to determine the "cut-off" frequency.

It should be noted that according to the proposed halo definition, even a matched beam with a thermal equilibrium distribution function has a certain fraction of halo particles. This fraction is exponentially small for a space-charge-dominated beam, but it increases with decreasing beam intensity since the half-value of the mismatch frequency approaches the frequency distribution of the betatron oscillators. Nevertheless, the spectral framework for a quantitative analysis of halo production developed above for a space-charge-dominated beam can also be efficiently utilized for the case of a low-intensity beam. The evolution of the beam betatron frequency distribution function due to beam mismatch relaxation for the case of a low-intensity beam with $\sigma^{sf}/\sigma_v^{sf} = 0.95$ ($s_b = 0.2$) is shown in Fig. 4. For this illustrative example, the beam mismatch is introduced in the same way as described above for the case of a space-charge-dominated beam, i.e., by increasing the focusing strength of the lattice to $\omega_q^{inc}/\omega_q = 1.3$ for a time period of $\tau_{\text{step}} = \pi/2(\omega_s^{sf})_i$. Comparing the betatron frequency distributions for the initial and final states [Fig. 4(a)], it is natural to assign a pronounced difference in the tail region where $\omega_{\beta x} > (\omega_s^{sf})_f/2$ to the generated beam halo. Note that for the case of an emittance-dominated beam, the mismatch oscillations are completely relaxed [Fig. 4(b)] and, therefore, particles do not experience a resonance interaction in the final state [compare Fig. 4(d) and Fig. 2(c)].

IV. EFFECTS OF AN ALTERNATING-GRADIENT QUADRUPOLE FIELD

The quantitative analysis of halo production by a beam mismatch developed above for a constant focusing field (smooth-focusing approximation) can be generalized in a straightforward manner to the case of an oscillating quadrupole focusing field. Figure 5(a) shows the evolution of the beam betratron frequency distribution function due to beam mismatch relaxation for the case of a space-charge-dominated beam with $\sigma/\sigma_{\text{vac}} = 0.25$ and $\sigma_{\text{vac}} = 55^0$. For this simulations, the initial beam distribution is loaded into a quadrupole lattice by making use of the pseudoequilibrium

procedure,[20] which provides an initial beam matching sufficient for present purposes. Then, a beam mismatch is introduced by an instantaneous increase in the lattice amplitude to $\hat{\kappa}_q^{inc}/\hat{\kappa}_q = 1.15$ at the zero phase of the sine function. The lattice amplitude is maintained fixed at $\hat{\kappa}_q^{inc}$ for one-half of the lattice period, and then instantaneously decreased to its initial value, $\hat{\kappa}_q$. This lattice perturbation provides the initial beam mismatch $\mu = 2.3$ as measured by the ratio of the maximum to minimum values of $X_{\rm rms} = \langle x^2 \rangle^{1/2}$ calculated at the end of each focusing cell within the first three periods of the smooth-focusing mismatch oscillations.

Note that the nonmonotonic tail structure in Fig. 5(a) is now represented by the two bumps corresponding to half-values of the symmetric (even), ω_s, and the quadrupole (odd), $\omega_{\rm odd}$, mismatched envelope mode frequencies (Sec. II). This is due to the fact that both modes are exited by the abrupt mismatch, and they both produce high-energy resonant halo particles. The quantitative criteria for a beam halo particle should therefore be generalized for the case of a quadrupole oscillating lattice in the following way: *if the particle betatron frequency is greater than the quadrupole (odd) envelope frequency half-value then it is designated as a halo particle*. To further investigate this criterion, we compare the normalized $(X, \dot{X})$ beam phase space shown in Fig. 5(c) with the same phase space after removing particles with betatron frequency satisfying $\omega_\beta > (\omega_{\rm odd}^{sf})_f/2$ [Fig. 5(d)]. Here, $(\omega_{\rm odd}^{sf})_f = (K_b/2R_{bf}^2 + \varepsilon_f^2/R_{bf}^4)^{1/2}$ is the corresponding smooth-focusing value of the quadrupole (odd) mismatched envelope mode frequency in the final beam state. The actual spectrum of the rms beam envelope x-dimension obtained in the particle-in-cell (PIC) simulations, taking into account the oscillating nature of the applied lattice and nonlinear effects, is shown in Fig. 5(b). Again, as noted earlier for the case of a constant focusing force (smooth-focusing approximation), a few more halo particles can be selected if an improved model accounting for the width and shape of the mismatch oscillations frequency spectrum is employed for determination of the cut-off frequency.

Finally, we present the evolution of the beam betatron frequency distribution due to mismatch relaxation for the case of a low-intensity beam, taking into account the effects of the oscillating applied lattice force (Fig. 6). For this illustrative example, we take $\sigma/\sigma_{\rm vac} = 0.95$, $\sigma_{\rm vac} = 40^0$, and the beam mismatch is introduced by an instantaneous increase in the lattice amplitude to $\hat{\kappa}_q^{inc}/\hat{\kappa}_q = 1.2$ at the zero phase of the sine function. The lattice amplitude is maintained fixed at $\hat{\kappa}_q^{inc}$ for one lattice period, and then instantaneously decrease to its initial value $\hat{\kappa}_q$. This lattice perturbation provides the initial beam mismatch $\mu = 2.0$ as measured by the ratio of the maximum to minimum values of $X_{\rm rms} = \langle x^2 \rangle^{1/2}$ calculated at the end of each focusing cell within the first three periods of the smooth-focusing mismatch oscillations. Inspecting the beam frequency distributions at the initial and final beam states, it again appears natural to assign a pronounced difference in the tail region for $\omega_{\beta x} > (\omega_{\rm odd}^{sf})_f/2$ to the generated beam halo.

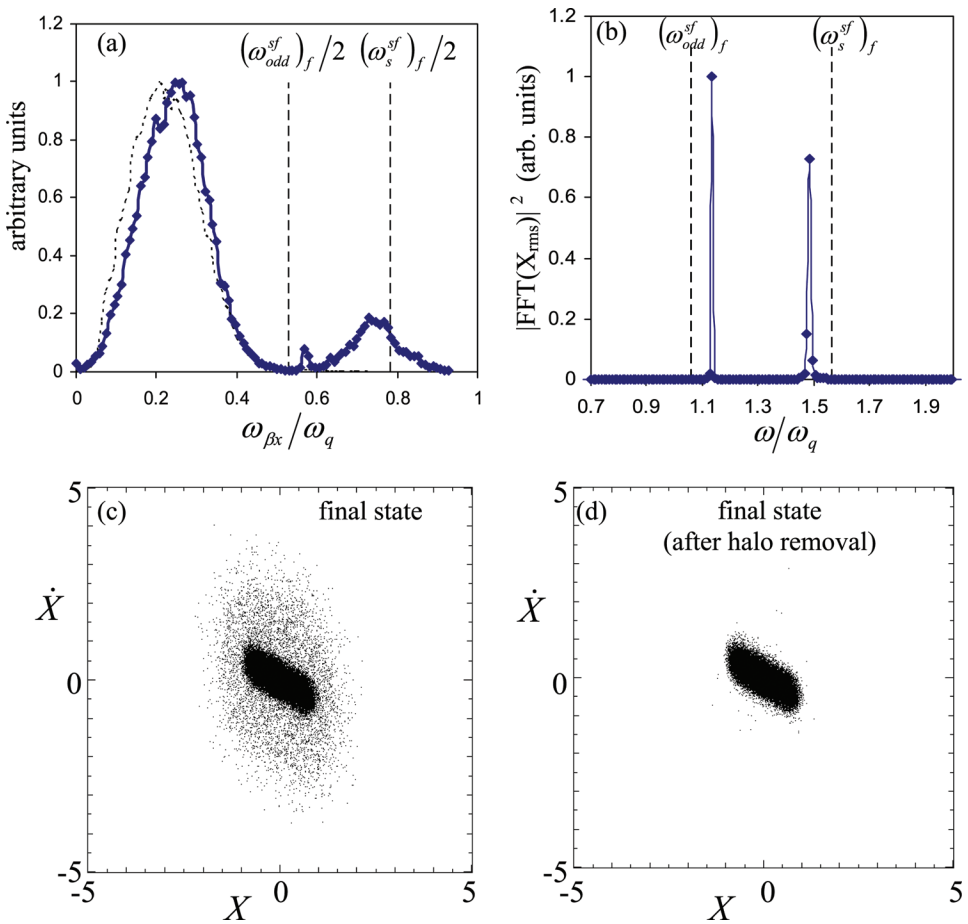

FIG. 5. (Color online) Relaxation of a beam mismatch for the case of a space-charge-dominated beam with $\sigma/\sigma_{\rm vac} = 0.25$ ($s_b = 0.9999$), $\sigma_v = 55^0$. Shown are plots of (a) beam betatron frequency distribution at the final quasirelaxed state (solid blue curve) and the initial state (dashed black curve); (b) fast-Fourier transform of $X_{\rm rms}(t)$; and (c) and (d) the instantaneous $(\dot{X}, X)$ phase space corresponding to the final state at $t = 325.9 \times 2\pi/\omega_q$ and the final state after halo removal, respectively. The time interval used for the FFT calculations of the betatron frequency distribution in the final state corresponds to $(220 \times 2\pi/\omega_q,\ 325 \times 2\pi/\omega_q)$. Results are obtained using the WARP code for an alternating-gradient quadrupole field.

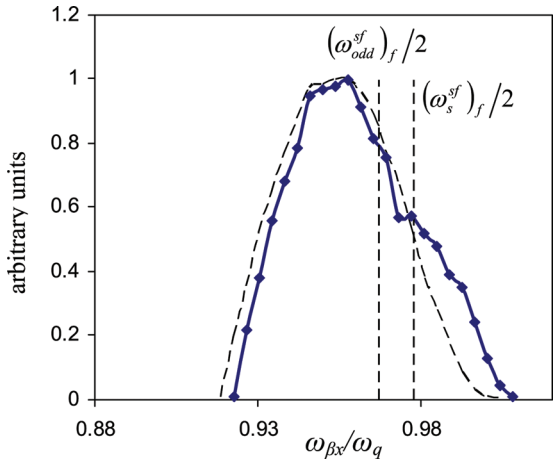

FIG. 6. (Color online) Evolution of the beam betatron frequency due to mismatch relaxation for the case of an emittance-dominated beam with $\sigma/\sigma_{vac} = 0.95$ ($s_b = 0.2$), $\sigma_{vac} = 40^0$. Shown are plots of the betatron frequency distribution at the final quasirelaxed state (solid blue curve) and at the initial state (dashed black curve). The time interval used for the FFT calculations of the betatron frequency distribution in the final state corresponds to $(161 \times 2\pi/\omega_q, 419 \times 2\pi/\omega_q)$. Results are obtained using the WARP code for an alternating-gradient quadrupole field.

V. SPECTRAL ANALYSIS OF STRONG MISMATCH RELAXATION AND INTENSE BEAM TRANSPORT LIMITS

The spectral analysis of a mismatched beam distribution has been demonstrated to be a powerful tool for studies of nonlinear transverse dynamics of an intense beam propagating through a periods-focusing lattice. In particular, it can provide the opportunity to carry out a quantitative analysis of halo production by a beam mismatch. In this section, we make use of this new formalism to study other critical problems in intense beam transport.

A. The spectral evolution of a beam core during the relaxation of a beam mismatch

In Sec. IV, the analysis was focused on beam halo production by a beam mismatch. However, it is also of particular interest to study the evolution of the beam core during the relaxation of a beam mismatch. Figure 7(a) shows the evolution of the beam betatron frequency distribution obtained within the smooth-focusing approximation for the case of a space-charge-dominated beam with $\left(\sigma^{sf}/\sigma_v^{sf}\right)_i = 0.25$. For this simulation, the mismatch was introduced by an instantaneous compression of the lattice amplitude to the value $\omega_{qf}/\omega_{qi} = 1.4$, which provided the initial beam mismatch $\mu = 2$ as measured by the ratio of the maximum to minimum values of R_b. Shown in Fig. 7(a) are the frequency distributions calculated at the time instants corresponding to $t_1 = 810.35 \times 2\pi/\omega_{qf}$ and $t_2 = 4350.35 \times 2\pi/\omega_{qf}$. It is interesting to note that the bump-on-tail structure in Fig. 7(a) attributed to the beam halo remains nearly the same, whereas the difference is clear in the core region. This means that most of the beam halo is generated on a time-scale shorter than the time-scale of the beam core evolution. Finally, we note that the core relaxation process also leads to an increase in the beam emittance. Figure 7(b) illustrates the evolution of the beam

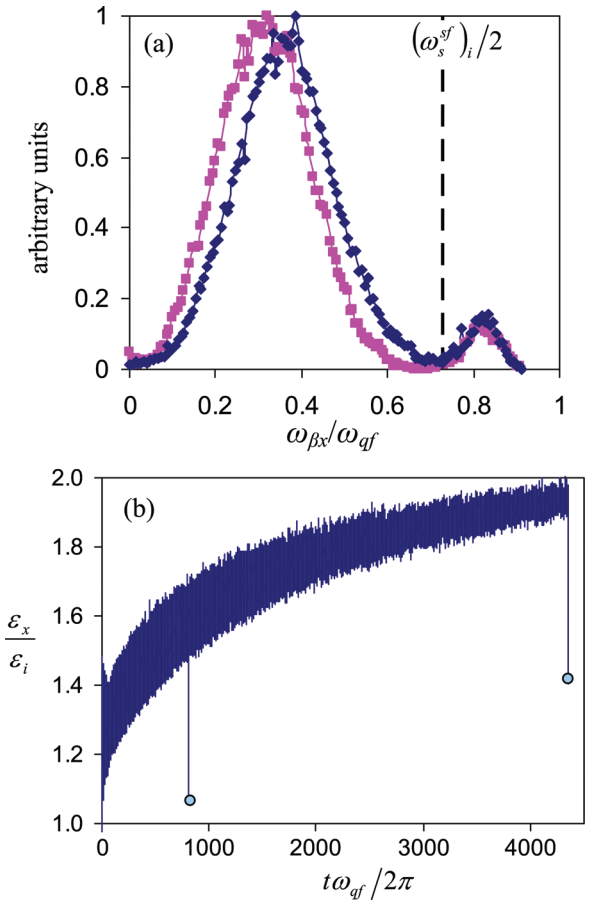

FIG. 7. (Color online) Strong mismatch relaxation for the case of a space-charge-dominated beam with $\sigma^{sf}/\sigma_v^{sf} = 0.25$ ($s_b = 0.9999$). Shown are plots of (a) the beam betatron density distribution function calculated at $t_1 = 810.35 \times 2\pi/\omega_{qf}$ (blue diamonds) and $t_2 = 4350.35 \times 2\pi/\omega_{qf}$ (pink squares) and (b) evolution of the beam transverse emittance. The dots illustrate the values of the beam transverse emittance at the time instants t_1 and t_2 when the halo particles are removed from the corresponding beam distributions. The beam mismatch is introduced by an instantaneous increase in the lattice strength to the value, $\omega_{qf} = 1.4\omega_{qi}$. The length of the time interval used for the FFT calculations of the betatron frequency distribution corresponds to $150 \times 2\pi/\omega_{qf}$. Results are obtained using the WARP code for a smooth-focusing force.

transverse emittance during the mismatch relaxation process. It is readily seen that the beam emittance continues to grow during the time period between t_1 and t_2, when most of the halo is generated. To further elucidate this, we compare the values of the beam emittance calculated at t_1 and t_2 after removing halo particles from the corresponding beam distributions. The corresponding values of the beam emittance calculated for the beam distributions without halo particles are shown by the dots in Fig. 7(b) and clearly demonstrate an increase in the beam emittance due to the beam core relaxation.

B. Spectral analysis of intense beam transport limits

Intense beam transport stability limits is one of the critical problems in intense beam transport. Of particular importance here are the higher-order resonance effects that limit stable intense beam propagation in the region of high vacuum phase advance, where[12–14]

$$\sigma_{vac}^2 - \sigma^2 \gtrsim (2\pi/3)^2/2. \tag{13}$$

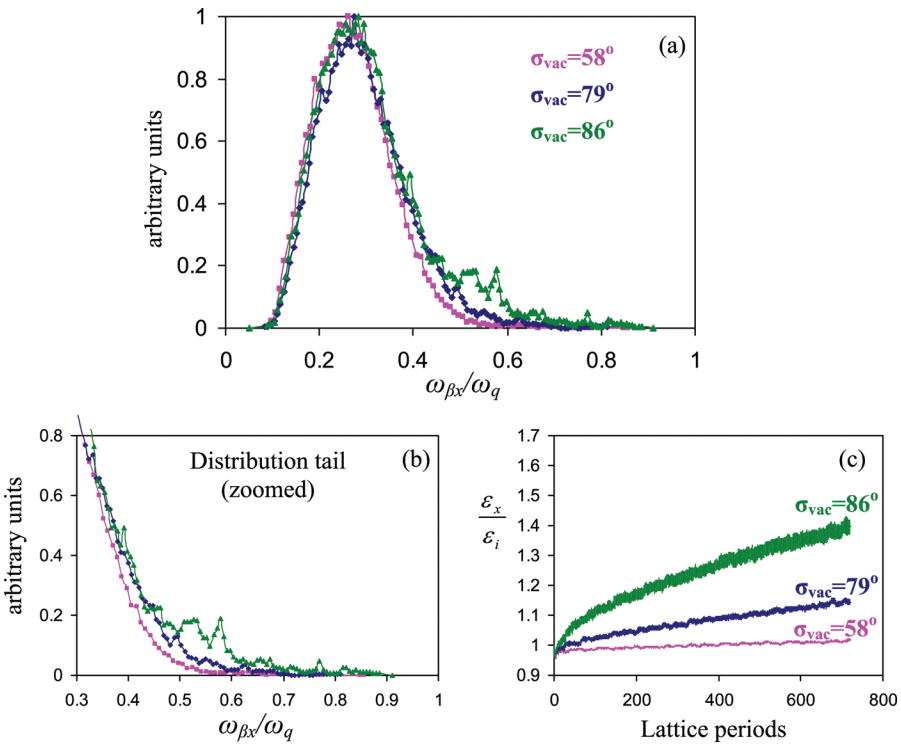

FIG. 8. (Color online) Dynamics of a space-charge-dominated beam with $\sigma/\sigma_v = 0.3$ in a quadrupole lattice for the cases where the system parameters approach the transport stability limit $\sigma_v^2 - \sigma^2 \cong (2\pi/3)^2/2$. Shown are plots of (a) the beam betatron distribution function for increasing values of the vacuum phase advance corresponding to $\sigma_v = 58^0$ (pink squares), $\sigma_v = 79^0$ (blue diamond), $\sigma_v = 86^0$ (green triangles); (b) zoom-in of the tails of the distributions shown in frame (a); and (c) evolution of the beam transverse emittance. The time interval used for the FFT calculations of the betatron frequency distributions corresponds to (0, 720 lattice periods). Results are obtained using the WARP code for an alternating-gradient quadrupole field.

In this section, we use the spectral analysis of the beam distribution to provide insights into that problem. The betatron frequency distributions for an intense beam with $\sigma/\sigma_{vac} = 0.3$ propagating through a quadrupole lattice are shown in Fig. 8(a) for different values of the lattice vacuum phase advance. Note that for $\sigma/\sigma_{vac} = 0.3$, the instability criteria [inequality (13)] can be expressed as $\sigma_{vac} \gtrsim 89^0$. The corresponding evolution of the beam transverse emittance is shown in Fig. 8(c), and a pronounced increase in the beam emittance is evident where the system parameters approach the stability limit. For these simulations, we load the particles with a semi-Gaussian distribution, which is a Gaussian distribution in $\dot{x}$ and $\dot{y}$ and has a uniform (step-function) density profile, into the matched envelope obtained from Eqs. (2) and (3). Finally, increased grid resolution corresponding to 64 grid points across the beam cross-section is used. It is evident from Figs. 8(a) and 8(b) that as the vacuum phase advance increases and the system parameters approach the instability criteria, the core of the betatron frequency distribution does not change significantly. However, the distribution tail function increases in extent. This observation supports the analysis developed in Ref. 14, which proposes that the emittance growth can be attributed to high-energy beam edge particles that diffuse outside of the beam core sufficiently to participate in the higher-order resonances, thereby, increasing the statistical beam area in the transverse phase space, i.e., the beam transverse emittance.

VI. CONCLUSIONS

A new spectral technique for the analysis of a mismatched intense beam propagating through an alternating-gradient lattice has been developed. It has been shown that the betatron frequency distribution of a mismatched intense beam has a bump-on-tail structure attributed to the beam halo particles. Based on this phenomenon, a quantitative definition of halo particles produced by a beam mismatch has been proposed, which provides an opportunity to carry out quantitative studies of halo particle production. It is also found that the analysis, based upon the spectral method, can provide important physical insights into other critical problems in intense beam transport, such as strong mismatch relaxation and space-charge transport limits. In particular, it has been demonstrated that during strong mismatch relaxation, most of the beam halo is generated on a time-scale shorter than the time-scale for the beam core relaxation. Furthermore, it has been observed that the core relaxation process also leads to an increase in the beam emittance. Finally, the spectral analysis of a beam distribution loaded into a quadrupole lattice for the case where the system parameters lie near the transport stability limit, $\sigma_{vac}^2 - \sigma^2 \approx (2\pi/3)^2/2$, has been performed. It has been shown that as the system parameters approach the stability limit, the core of the beam betatron distribution does not change significantly, whereas the tail of the distribution increases. This observation supports the analysis developed in Ref. 14, which proposed that the emittance growth can be attributed to high-energy beam edge particles that diffuse outside the beam core sufficiently to participate in the higher-order resonances, thereby increasing the statistical beam area in transverse phase space.

ACKNOWLEDGMENTS

This research was supported by the U.S. Department of Energy under Contract No. DE-AC02-76CH-O3073 with the Princeton Plasma Physics Laboratory.

[1]R. C. Davidson and H. Qin, *Physics of Intense Charged Particle Beams in High Energy Accelerators* (World Scientific, Singapore, 2001).

[2]R. L. Gluckstern, Phys. Rev. Lett. **73**, 1247 (1994).
[3]C. K. Allen, K. C. D. Chan, P. L. Colestock, K. R. Crandall, R. W. Garnett, J. D. Gilpatrick, W. Lysenko, J. Qiang, J. D. Schneider, M. E. Schulze, R. L. Sheffield, H. V. Smith, and T. P. Wangler, Phys. Rev. Lett. **89**, 214802 (2002).
[4]T. P. Wangler, K. R. Crandall, R. Ryne, and T. S. Wang, Phys. Rev. ST Accel. Beams **1**, 084201 (1998).
[5]J. Qiang, P. L. Colestock, D. Gilpatrick, H. V. Smith, T. P. Wangler, and M. E. Schulze, Phys. Rev. ST Accel. Beams **5**, 124201 (2002).
[6]K. G. Sonnad and J. R. Cary, Phys. Rev. ST Accel. Beams **8**, 064202 (2005).
[7]H. Okamoto and M. Ikegami, Phys. Rev. E **55**, 4694 (1997).
[8]M. Dorf, R. C. Davidson, and E. Startsev, Phys. Rev. ST Accel. Beams **9**, 034202 (2006).
[9]M. Dorf, R. C. Davidson, and E. Startsev, in *Proceedings of the Particle Accelerator Conference*, Albuquerque, NM, 2007 (IEEE, Piscataway, NJ 2007), p. 3669.
[10]T. P. Wangler and K. R. Crandall, in *Proceedings of the 20th International Linac Conference*, *Monterey, 2000*, edited by A. Chao, eConf C000821, 2000, p. 341.
[11]C. K. Allen and T. P. Wangler, Phys. Rev. ST Accel. Beams **5**, 124202 (2002).
[12]M. G. Tiefenbach and D. Keefe, IEEE Trans. Nucl. Sci. **32**, 2483 (1985).
[13]M. G. Tiefenbach, "*Space-Charge Limits on the Transport of Ion Beams*" Ph.D. thesis University of California, Berkeley, CA, 1986; Lawrence Berkeley Lab Report No. LBL-22465, 1986.
[14]S. M. Lund and S. R. Chawla, Nucl. Instrum. Methods Phys. Res. A **561**, 203 (2006).
[15]M. Reiser, *Theory and Design of Charged Particle Beams* (Wiley, New York, 1994).
[16]T. Clauser, V. Stagno, and V. Variale, in *Proceedings of the Particle Accelerator Conference*, New York, 1999 (IEEE, Piscataway, NJ, 1999), p. 1779.
[17]V. Variale, Phys. Rev. ST Accel. Beams **4**, 084201 (2001).
[18]D. P. Grote, A. Friedman, I. Haber, W. Fawley, and J.-L. Vay, Nucl. Instrum. Methods Phys. Res. A **415**, 428 (1998).
[19]E. A. Startsev and S. M. Lund, Phys. Plasmas **15**, 043101 (2008).
[20]S. M. Lund, T. Kikuchi, and R. C. Davidson, Phys. Rev. ST Accel. Beams **12**, 114801 (2009).